Vera Pavlova* and Elena Murashova

New compound $Sm_2Ru_3Sn_5$ with a structure derived from Ru_3Sn_7

https://doi.org/10.1515/zkri-2021-2013
Received February 2, 2021; accepted May 11, 2021;
published online May 31, 2021

Abstract: Ternary intermetallic compound $Sm_2Ru_3Sn_5$ was synthesized in the system Sm-Ru-Sn by arc-melting and annealing at 600 °C in the field with high content of Sn. Its crystal structure was determined using single crystal X-ray diffraction data (at 240 K). The compound crystallizes in cubic system with space group $I\bar{4}3m$ (No. 217), unit cell parameter is a = 9.4606 (8) Å, Z = 4, Pearson symbol c/40. The intermetallic compound $Sm_2Ru_3Sn_5$ represents an ordered version of the centrosymmetric Ru_3Sn_7 structure (space group $Im\bar{3}m$), in which 16*f* Sn-filled crystallographic site is split into two 8*c* sites, each of which is solely occupied of one sort of atoms – Sn or Sm. The occupation of these two 8*c* sites leads to a reduction of symmetry due to the removal of the inversion center.

Keywords: arc-melting; stannide; crystal chemistry; scanning electron microscopy; intermetallics; X-ray diffraction.

1 Introduction

Ternary intermetallic compounds of composition $RE_2T_3X_5$ (RE – rare earth metals, T – transition element, X – Si, Ge, Ga, In, Sn) are being intensively studied due to their unusual magnetic and electrical properties, namely, superconductivity ($Lu_2Fe_3Si_5$ T_c = 6 K [1], $Pr_2Pt_3Ge_5$ T_c = 8 K [2], $Tm_2Fe_3Si_5$ T_c = 1.7 K [3], $Lu_2Ir_3Si_5$ T_c = 3.5 K [4]), mixed-valence state ($Ce_2Ni_3Si_5$ [5], $Eu_2Pt_3Si_5$ [6], $CaYbPt_3Sn_5$ [7], $Ce_2Rh_3Si_5$ [8], $Ce_2Ir_3Si_5$ [9]), heavy fermion behaviour ($Pr_2Rh_3Ge_5$ [10], $Yb_2Fe_3Si_5$ [11]), unusually large magnetoresistance ($Pr_2Pd_3Ge_5$ [10]), antiferromagnetically ordered dense Kondo systems ($Ce_2Rh_3Ge_5$, $Ce_2Ir_3Ge_5$ [12]), ferromagnetic ordering behaviour ($Pu_2Pt_3Si_5$ [13]) and others.

$RE_2T_3X_5$ intermetallics exhibit a wide diversity of crystal structures. They crystallize in the six structural types: (1) $U_2Mn_3Si_5$ (*P*4/*mnc*) a = 10.57 Å, c = 5.435 Å [14]; (2) $U_2Co_3Si_5$ (*Ibam*) a = 9.59 Å, b = 11.13 Å, c = 5.617 Å [15]; (3) $Lu_2Co_3Si_5$ (*C*2/*c*) a = 10.640 Å, b = 11.358 Å, c = 5.432 Å, β = 118.37° [16]; (4) $Y_2Rh_3Sn_5$ ($Cmc2_1$) a = 4.387 Å, b = 26.212 Å, c = 7.1550 Å [17]; (5) $Yb_2Pt_3Sn_5$ (*Pnma*) a = 7.295 Å, b = 4.422 Å, c = 26.252 Å [7, 18]; (6) $Ce_2Au_3In_5$ ($Pmn2_1$) a = 4.6527 Å, b = 53.483 Å, c = 7.405 Å [19, 20]. The distribution of ternary compounds of $RE_2T_3X_5$ by structural types was considered by D. Bugaris et al. in [21]. According to this paper, more than half of the $RE_2T_3X_5$ compounds are of type $U_2Co_3Si_5$, while structural type $U_2Mn_3Si_5$ includes a quarter of compounds of this composition. The third structural type, $Lu_2Co_3Si_5$, which is a distortion variant of $U_2Co_3Si_5$ type, includes about 20 compounds. The remaining three structural types include a few (13) compounds with a relatively large *X* component – In, Sn, or Bi. The crystal chemical relationship of the structural types $Y_2Rh_3Sn_5$, $Yb_2Pt_3Sn_5$, and $Ce_2Au_3In_5$ is discussed in detail by *Y*. Galadzhun et al. in Ref. [19]. According to [19], all three structure types have the common supergroup *Cmcm*, and the differences between these types result from different ordering of the transition metal and tin or indium atoms within the polyanionic network.

In the process of studying the Sm-Ru-Sn system, we discovered a compound of the $Sm_2Ru_3Sn_5$ composition with a new type of crystal structure. Previously, only two ternary compounds were found in this system: $SmRuSn_3$, which demonstrates the antiferromagnetic ordering at T_N = 6 K and the valence fluctuation of Sm atoms [22–24] and $SmRu_4Sn_6$ [25], which exhibits the antiferromagnetic ordering at T_N = 8.3 K [26]. Unlike Sm-Ru-Sn system, stannides with rhodium $RE_2Rh_3Sn_5$ and a set of rare earths, including samarium (RE = Y, Ce-Nd, Sm, Gd-Tm), have been studied in more detail [17, 27, 28]. Their structures belong to the structural type $Y_2Rh_3Sn_5$ ($Cmc2_1$). $Sm_2Rh_3Sn_5$ demonstrates antiferromagnetic ordering at T_N = 3.5 K [27]. In the crystal structure of $Ce_2Rh_3Sn_5$, Ce ions occupy two different lattice positions, which leads to two antiferromagnetic ordering (T_{N1} = 2.9 K, T_{N2} = 2.4 K). Moreover, the

***Corresponding author: Vera Pavlova**, Chemistry Department, Lomonosov Moscow State University, Moscow 119991, Russia, E-mail: veragriban@gmail.com
Elena Murashova, Chemistry Department, Lomonosov Moscow State University, Moscow 119991, Russia

compound demonstrate the coexistence of magnetic order and valence fluctuations of Ce ions in the Kondo lattice [28]. $Tm_2Rh_3Sn_5$ is a superconductor below 1.8 K [29].

In this paper, we present the information about the synthesis, crystal structure and its features for the novel ternary stannide of samarium and ruthenium – $Sm_2Ru_3Sn_5$.

2 Experimental section

2.1 Synthetic procedures

The sample $Sm_{20}Ru_{30}Sn_{50}$ (at.%) was synthesized by arc-melting from the pure elements Sm (99.9 mass% Sm), Ru (99.99 mass% Ru), Sn (99.999 mass% Sn) in a purified argon atmosphere. To reach the homogeneity the fused mass was re-melted several times. The alloy was annealed at 600 °C for 30 days after melting. The annealing temperature was selected on the basis of the analysis of the phase diagram of binary systems Sm-Ru [30, 31], Ru-Sn [32] and Sm-Sn [33]. The total mass lost wasn't higher than 1% of weight.

2.2 X-ray single crystal diffraction (XRSCD)

The suitable single crystal for X-ray structure analysis was found at the surface of the annealed alloy $Sm_{20}Ru_{30}Sn_{50}$ (at.%). X-ray single crystal diffraction experiment was performed using Bruker APEX3 diffractometer employed monochromated MoK_α radiation (λ = 0.71073 Å) at 240 K. All obtained intensities were collected and derived using the program Bruker Saint [34]. Absorption correction was performed with the SADABS program [35]. The structure was solved by direct methods and refined with the Shelx-2018 program package [36].

2.3 X-ray powder diffraction (XRD)

X-ray powder diffraction data were collected using of STOE STADI *P* transmission diffractometer (monochromated $CuK_{\alpha 1}$ – radiation (λ = 1.54056 Å), 10° < 2θ < 89.99°, linear position-sensitive detector, step scan 0.01° and counting time 10 s/point). Indexing the XRD pattern and lattice parameters determination were done using Treor program included in the Stoe Winxpow package [37]. Quantitative refinement of the powder X-ray pattern by Rietveld method was performed with the Fullprof program [38, 39], employing internal tables for X-ray atomic form factors. Structure and atom polyhedra were visualized using the Diamond program [40].

2.4 Scanning electron microscopy (SEM) and energy dispersive X-ray spectroscopy (EDX analysis)

Microstructure and chemical composition of the prepared alloy was established by scanning electron microscopy and by energy dispersive X-ray spectroscopy using Carl Zeiss LEO EVO 50VXP microscope equipped with an INCA Energy 450 EDX-spectrometer (Oxford Instruments). Accelerating voltage was 20 kV. The measurement error did not exceed 1 at.%.

3 Results and discussion

3.1 Sample characterization

EDX analysis revealed the overall chemical composition of the prepared as cast alloy to be close to $Sm_{20}Ru_{30}Sn_{50}$ (at.%). The sample contained three phases: new main phase $Sm_2Ru_3Sn_5$ with the measured composition $Sm_{19}Ru_{30}Sn_{51}$ (at.%), Ru (Ru_{99} (at.%)), and $SmRuSn_3$ ($Sm_{19}Ru_{20}Sn_{61}$ (at.%)) [23]. The microstructure of the as cast sample is presented in Figure 1a. After the heat treatment of the ingot, no other phases were detected by EDX analysis besides $Sm_2Ru_3Sn_5$ and Ru. The content of the $SmRuSn_3$ phase was so small that it was missing on the microstructure of the sample (Figure 1b). However, according to results of XRD analysis the presence of three phases, Ru, $Sm_2Ru_3Sn_5$ and $SmRuSn_3$, in annealed ingot was proven.

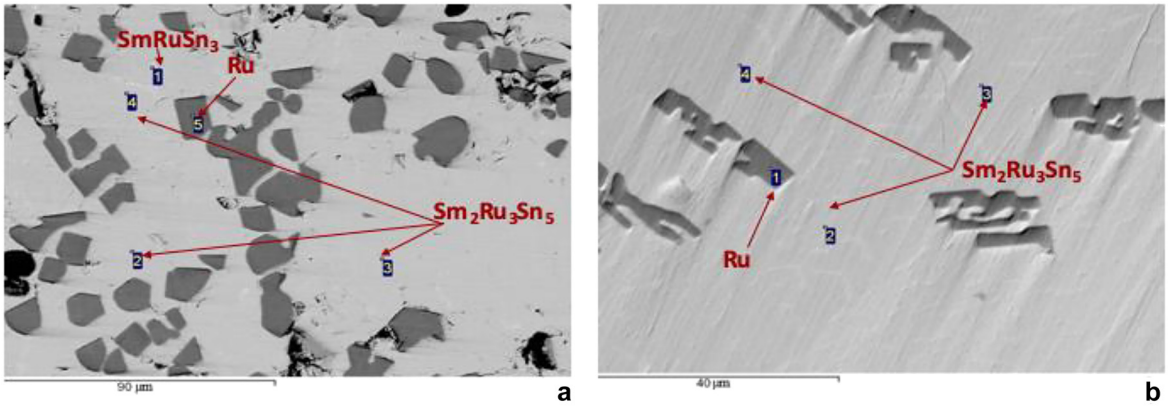

Figure 1: Microstructure of the as cast (a) and annealed (b) $Sm_{20}Ru_{30}Sn_{50}$ (at.%) ingot, obtained on a scanning electron microscope. Marked are the measured points.

3.2 Crystal structure description

According to XRD powder data, the new compound crystallizes in the cubic system and the unit cell parameter $a = 9.4540(1)$ Å $F_{30} = 64.1$ (Treor [37]). This parameter and the distribution of diffraction intensities indicate a close resemblance with the well-known binary compound Ru_3Sn_7 (space group $Im\bar{3}m$) [41, 42]. The determination of the crystal structure of $Sm_2Ru_3Sn_5$ was carried out on a single crystal selected from the surface of a destroyed annealed sample. The structure model of the new $Sm_2Ru_3Sn_5$, obtained by direct methods and refined using the Shelx program, has non-centrosymmetric space group $I\bar{4}3m$. The absence of inversion center in the structure of $Sm_2Ru_3Sn_5$ was ensured with use of Platon program [43]. Refinement of the occupancy of the crystallographic sites for all atoms indicated no deviation from the ideal composition. To confirm the structural model obtained from the XRSCD data and to determine the content of impurity phases in the annealed ingot, the Rietveld refinement of powder pattern was carried out. The ordered distribution of Sm and Sn atoms in the structure with non-centrosymmetric space group $I\bar{4}3m$ leads to the best result (Figure 2). In the calculations, apart from the major cubic phase of $Sm_2Ru_3Sn_5$ (80 wt%), the contributions due to Ru (15 wt%) and $SmRuSn_3$ (5 wt%) impurity phases were taken into account. The refined experimental and theoretical patterns have good match of reflections (Figure 2 and Table 1). The final Rietveld refinement resulted in $R_F = 0.013$, $R_B = 0.017$, $\chi^2 = 1.47$. The main crystallographic details of the data collection and evaluation are presented in Table 1. Atomic coordinates and displacement parameters are summarized in Table 2, while the interatomic distances are given in Table 3. Further details of the crystal structure investigation may be obtained from CCDC/FIZ Karlsruhe, 76344 Eggenstein-Leopoldshafen, Germany (Fax: +49-7247-808-666; E-mail: crysdata@fiz-karlsruhe.de), on quoting the deposition number CSD-1942140.

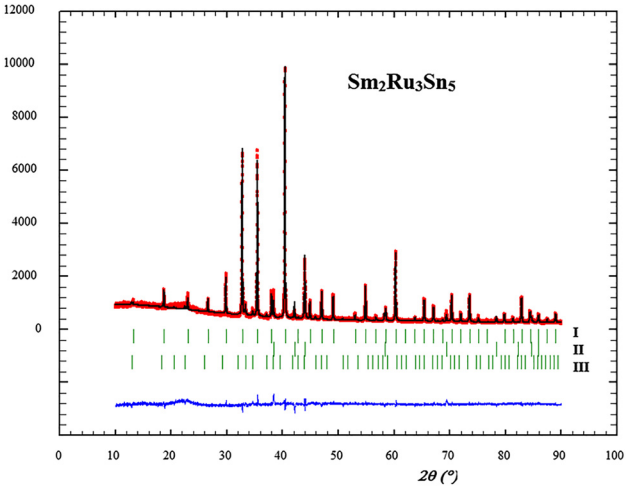

Figure 2: Experimental powder diffraction pattern (red circles), calculated diffraction pattern (black solid line), and the difference curve (bottom blue line) for an ingot $Sm_{20}Ru_{30}Sn_{50}$ (at.%) analyzed in terms of Rietveld refinement. The content of three phases: I – $Sm_2Ru_3Sn_5$ (80 wt%), II – Ru (15 wt%), III – $SmRuSn_3$ (5 wt%).

Intermetallic compound $Sm_2Ru_3Sn_5$ crystallizes in the cubic unit cell, space group $I\bar{4}3m$, lattice parameter a = 9.4606(8) Å (single crystal data). In the unit cell of $Sm_2Ru_3Sn_5$, atoms are located in four non-equivalent positions: Sm (8*c*), Ru (12*e*), Sn1 (12*d*), Sn2 (8*c*). Figure 3 demonstrates the projection of the unit cell of $Sm_2Ru_3Sn_5$ along the direction [001].

A samarium atom is surrounded by 13 atoms at a distance up to 3.45 Å (3Ru + 4Sn2 + 6Sn1) forming distorted hexagonal prism with one additional atom (coordination number (CN), CN = 13, Figure 3a). Six tin atoms (2Sn2 + 4Sn1) and additional two samarium and one ruthenium atoms (2Sm + Ru) form a three-cap trigonal prism around ruthenium atom at a distance up to 3.03 Å (CN = 9, Figure 3b). Sn1 atom occupies the center of a strongly distorted cuboctahedron (4Sm + 4Ru + 4Sn1) formed by atoms at a distance of up to 3.45 Å (CN = 12, Figure 3c). The bases of the cuboctahedron are strongly elongated rhombuses [2Ru + 2Sn1] lying in parallel planes and rotated 90° relative to each other (Figure 3d). For greater clarity, this polyhedron is shown twice in Figure 3(c and d). Sn2 atom is located inside a 10-vertexes polyhedron (4Sm + 3Ru + 3Sn2) (CN = 10, Figure 3e). Interatomic distances of Sn2 with atoms forming the coordination polyhedron do not exceed 3.21 Å.

The cubic structure of $Sm_2Ru_3Sn_5$ could be presented as a derivative from the structure of known binary compound of Ru_3Sn_7 [41, 42], which crystallizes with the cubic centrosymmetric space group $Im\bar{3}m$, unit cell parameter a = 9.3735 Å [42], own type of structure [41]. In the literature, this type of structure is also referred to as a Ir_3Ge_7 type [44]. In the unit cell of Ru_3Sn_7, atoms are distributed over three non-equivalent positions: Ru (12*e*), Sn1 (12*d*), and Sn2 (16*f*). In the $Sm_2Ru_3Sn_5$ structure, there is a loss of the inversion center and splitting of the 16*f* position into two 8*c* positions, one of which contains samarium atoms, and the other contains tin atoms. Beside Ru_3Sn_7, the unit cell of $Sm_2Ru_3Sn_5$ structure is similar to the body centered cubic unit cell of the ternary $Nb_3Sb_2Te_5$. Its structure, established before in [45], was assigned to the Ir_3Ge_7 structural type, a cubic system, space group $Im\bar{3}m$ with mixed Sb/Te positions. Authors of [45] noted the statistical distribution of Sb

Table 1: Crystallographic data and structure refinement parameters for $Sm_2Ru_3Sn_5$ from the single crystal and powder X-ray diffraction intensities.

XRD data	Single crystal	Powder
Composition, EDX, at.%	$Sm_{19}Ru_{30}Sn_{51}$	
Formula	$Sm_2Ru_3Sn_5$	
Molar mass (g/mol)	1197.36	
Space group	$I\bar{4}3m$ (No. 217)	
Formula units, Z	4	
Crystal system, Pearson symbol	Cubic, $cI40$	
T (K)	240(2)	295(2)
Crystal size, mm	0.06 × 0.04 × 0.04	
a, (Å)	a = 9.4606(8)	a = 9.4540(1)
V, (Å^3)	V = 846.8(2)	V = 844.98(1)
Calculated density (g/cm^3)	9.39	9.41
Radiation, λ (Å)	MoK_α; 0.71073	$CuK_{\alpha1}$; 1.540598
Absorption coefficient (mm^{-1})	33.2	
F (000)	2024	
2θ range (min, max, °)	6.090, 61.632	10.00, 89.99, step 0.01
Range in h, k, l	−13–9, −13–13, −13–13	
Number of total reflections	3986	53
Number of independent reflections (R_{int})	280 (0.053)	
Number of reflections with $I > 2\sigma(I)$ (R_σ)	277 (0.021)	
Number of refined parameters	13	25*
Goodness-of-fit on F^2	1.151	
Final $R1$ [$I > 2\sigma(I)$]/all data	0.043/0.044	
w$R2$/all data	0.113/0.114	
Largest diff. peak/hole, e/Å^{-3}	2.43/−1.88	
Absolute structure parameter	−0.04(4)	
$R_P = \Sigma\lvert y_{oi} - y_{ci}\rvert/\Sigma\lvert y_{oi}\rvert$	–	0.037
$R_{wP} = [\Sigma w_i\lvert y_{oi} - y_{ci}\rvert^2/\Sigma w_i\lvert y_{oi}\rvert^2]^{1/2}$	–	0.058
$R_F = \Sigma\lvert F_{oi} - F_{ci}\rvert/\Sigma F_{oi}$	–	0.013
$R_B = \Sigma\lvert I_{o,h} - I_{c,h}\rvert/\Sigma\lvert I_{o,h}\rvert$	–	0.017
$\chi^2 = (R_{wP}/R_e)^2$	–	1.47

*Refined parameters include 9 structural and 16 profile parameters.

Table 2: Atomic coordinates, equivalent isotropic displacement parameters (Å$^2 \times 10^3$), and anisotropic displacement parameters (Å$^2 \times 10^3$) for $Sm_2Ru_3Sn_5$ (single crystal XRD).

Atom	Wyckoff position	x/a	y/b	z/c	U_{eq}	U_{11}	U_{22}	U_{33}	U_{23}	U_{13}	U_{12}
Sm	8c	0.2008(2)	x	x	17(1)	17(1)	17(1)	17(1)	−1(1)	−1(1)	−1(1)
Sn1	12d	1/4	0	1/2	17(1)	14(1)	19(1)	19(1)	0	0	0
Sn2	8c	0.3841(2)	x	x	16(1)	16(1)	16(1)	16(1)	0(1)	0(1)	0(1)
Ru	12e	1/2	0.1503(3)	1/2	15(1)	16(1)	13(1)	16(1)	0	3(1)	0

atoms into two sites 12d and 16f. Then, its structure was solved by a single crystal experiment and reported in [46]. It was proved that $Nb_3Sb_2Te_5$ crystallizes in a cubic cell with a = 9.8180 Å and belongs to the structure type derived from Ir_3Ge_7. The refinement of the structure in a non-centrosymmetric space group $I\bar{4}3m$, where former position 16f is split into two 8c sites, demonstrates an ordered variant of the structure in which the Sb and Te atoms are placed in 8c positions each. Since the Sb and Te atoms are close in size (1.59 Å and 1.60 Å respectively [47]), their atomic positions (x (Te2) = 0.166, x (Sb2) = 0.837) almost do not differ from the position in the centrosymmetric version of the structure (x (Te/Sb) = 0.165), and as a result, their nearest coordination environments are the same and similar to those in the prototype structure. Similar to $Nb_3Sb_2Te_5$, in the non-centrosymmetric crystal structure of novel $Sm_2Ru_3Sn_5$ three sorts of atoms are orderly distributed among the same four crystallographic sites of $I\bar{4}3m$

Table 3: Selected interatomic distances (Å) in the $Sm_2Ru_3Sn_5$ structure (single crystal data).

Atom 1	Atom 2	Distance
Sm	Sn2	3.004(5)
	3 Ru	3.0339(19)
	3 Sn2	3.204(3)
	6 Sn1	3.4405(7)
Sn1	4 Ru	2.7594(16)
	4 Sn1	3.3448(2)
	4 Sm	3.4407(7)
Sn2	3 Ru	2.702(3)
	Sm	3.004(5)
	3 Sn2	3.100(6)
	3 Sm	3.204(3)
Ru	2 Sn2	2.702(3)
	4 Sn1	2.7594(16)
	Ru	2.843(6)
	2 Sm	3.0339(19)

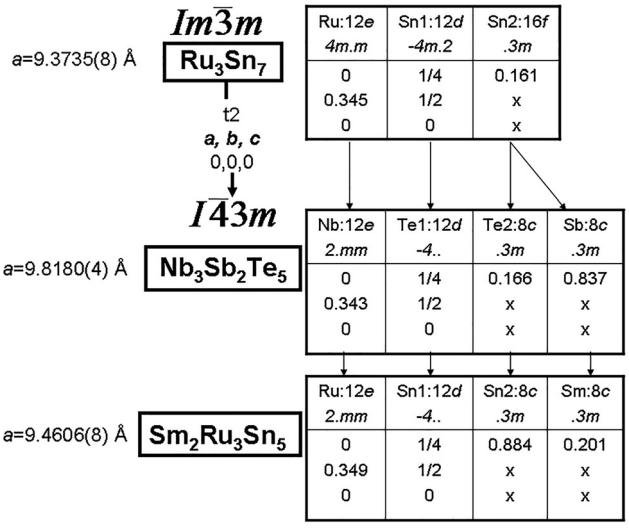

Figure 4: The transformation between structures Ru_3Sn_7, $Nb_3Sb_2Te_5$, and $Sm_2Ru_3Sn_5$ within the group-subgroup relations.

group (12*d*, 12*e* and two 8*c*). An important difference between these structures is that in $Sm_2Ru_3Sn_5$, the 8*c* positions are filled with atoms of very different sizes (Sn and Sm), while in $Nb_3Sb_2Te_5$, they are almost identical (Sb and Te). This feature leads to noticeable changes in the nearest environment of atoms.

The transformations between the Ru_3Sn_7, $Nb_3Sb_2Te_5$, and $Sm_2Ru_3Sn_5$ structures are presented in Figure 4 within the concept of group-subgroup relations in the Bärnighausen formalism [48, 49]. From the diagram in Figure 4, it can be seen that the difference in the coordinates of the Te and Sb atoms in the $Nb_3Sb_2Te_5$ structure is insignificant, and on the contrary, in the $Sm_2Ru_3Sn_5$ structure it is pronounced.

All these structures can be represented as a collection of infinite chains, which consist of empty convex eight-vertex polyhedra in a form of distorted tetragonal prism and pair of interconnected distorted tetragonal antiprisms with ruthenium (or niobium) atom inside (Figure 5a–c). In case of Ru_3Sn_7 and $Nb_3Sb_2Te_5$, empty tetragonal prisms are practically cubes of [Sn_8] (Figure 5a) and of [Sb_4Te_4] (Figure 5b), in case $Sm_2Ru_3Sn_5$, empty eight-vertex polyhedra are transformed into strongly distorted tetragonal prisms with corrugated rhombus-like bases (Figure 5c). The atoms forming the bases do not lie in the same plane, the maximum deviation of the atoms from each other is 0.804 Å (Figure 5c). The adjacent parallel chains are connected to each other by atoms (Sn-Sn, Sb-Te, Sm-Sn respectively) at distances, which slightly exceed the sum of the covalent radii of the atoms forming them. In the

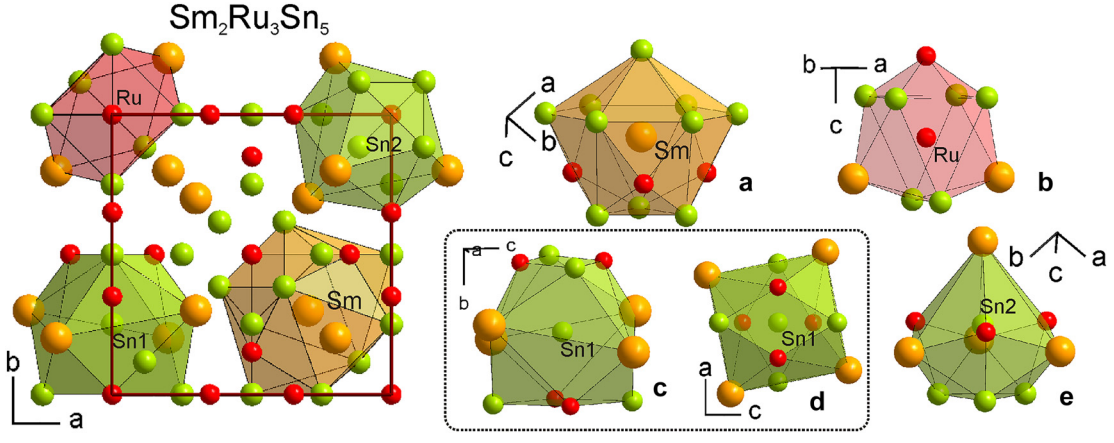

Figure 3: Projection of the unit cell of $Sm_2Ru_3Sn_5$ on the *ab*-plane with the coordination polyhedra as they are in the cell (left part). For better clarity the coordination polyhedra of the atoms are also presented in the other orientation: Sm (a), Ru (b), Sn1 (twice, c and d), and Sn2 (e) (right part).

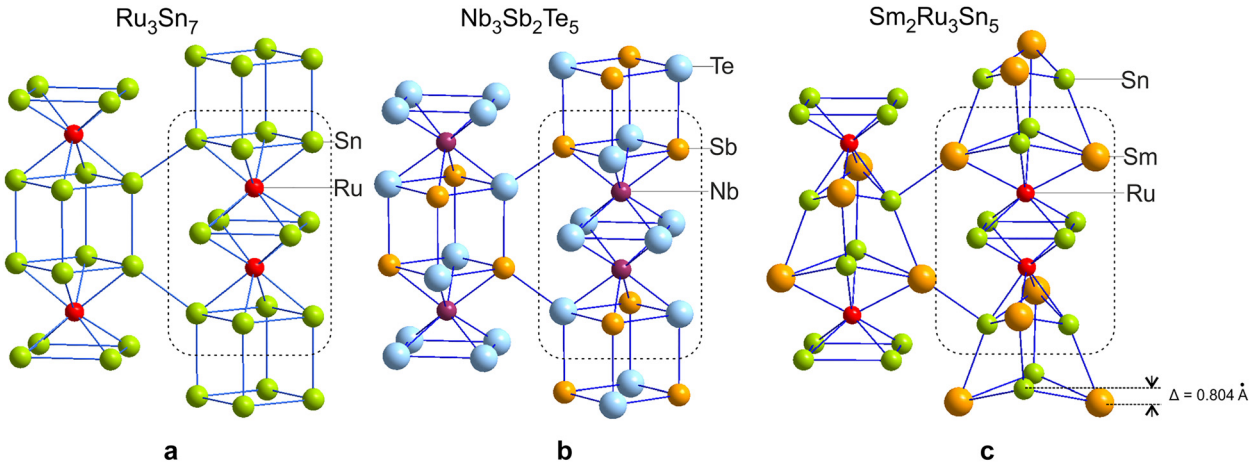

Figure 5: Two interconnected chains consisting of empty convex eight-vertex polyhedra [Sn_8] and pair of 2Ru[Sn_{12}] interconnected antiprisms in Ru_3Sn_7 (a), two interconnected chains consisting of empty convex eight-vertex polyhedra [Sb_4Te_4] and pair of 2Nb[Sb_4Te_8] interconnected antiprisms in $Nb_3Sb_2Te_5$ (b); two interconnected chains consisting of empty convex eight-vertex polyhedra [Sm_4Sn_4] and pair of 2Ru[Sm_4Sn_8] interconnected distorted antiprisms in $Sm_2Ru_3Sn_5$ (c). Pair of Ru (or Nb) antiprisms are outlined with a dashed lines.

$Sm_2Ru_3Sn_5$ structure, the two 8*c* positions are occupied by Sm and Sn atoms, which differ significantly in size (1.80 Å (Sm), 1.40 Å (Sn) [47]) and electronic structure, which leads to the formation of an environment around these atoms that differs from the environment of the corresponding atoms in Ru_3Sn_7 and $Nb_3Sb_2Te_5$.

The changes of the coordination polyhedra in Ru_3Sn_7, $Nb_3Sb_2Te_5$, and $Sm_2Ru_3Sn_5$ structures can be traced in Figures 5 and 6. The nearest environment of Ru (12*e*) atom in the Ru_3Sn_7 and Nb (12*e*) atom in the $Nb_3Sb_2Te_5$ structures is similar. In the both structures, atoms in 12*e* position have coordination number 9 (CN = 9) formed a tetragonal antiprism with one additional atom. In the Ru_3Sn_7, eight tin and one ruthenium atoms [Ru + 8Sn] are the vertices of Ru-polyhedron (Figures 5a, 6a). The opposite bases of the antiprism are parallel to each other. The interatomic distances between the central atom and the vertices in the Ru-polyhedron in the Ru_3Sn_7 structure take two values that are close to each other: 2.75 and 2.76 Å, while Ru-Ru distance is little bigger 2.90 Å. Analogously in the $Nb_3Sb_2Te_5$, Nb atom is surrounded by six tellurium atoms, two antimony atoms and one niobium atom (as a cap) (Nb + 6Te + 2Sb) forming a one-cap tetragonal antiprism (Figure 5b). The distances between the central atom and vertices Nb-Sb (2.87 Å) Nb-Te (2.89 Å, 2.90 Å) in the polyhedron are almost identical.

Other coordination polyhedra in the $Nb_3Sb_2Te_5$ structure are also similar to these in the Ru_3Sn_7 structure. On the contrary, in the structure of $Sm_2Ru_3Sn_5$, due to the introduction of the larger Sm atoms, the immediate environment of the atoms undergoes changes. The ruthenium polyhedron is transformed from a tetragonal one-cap antiprism to a trigonal three-cap prism. Figure 6a shows how one of the square bases of the Ru-antiprism in the Ru_3Sn_7 structure turns into an elongated rhombus with a break in the $Sm_2Ru_3Sn_5$ structure. In this situation, the polyhedron is more correctly described as a trigonal three-cap prism, where the caps are two samarium atoms and one ruthenium atom (Figure 6b).

The most significant changes are observed in the immediate environment of the Sn2 (8*c*) and Sn1 (12*d*) atoms in the $Sm_2Ru_3Sn_5$ structure compared to the environment of the Sn2 (16*f*) and Sn1 (12*d*) atoms in Ru_3Sn_7. In the Ru_3Sn_7 and $Sm_2Ru_3Sn_5$ structures, the coordination environment of Sn1 (12*d*) atom in the form of a tetragonal antiprism [4Ru4Sn] is similar only within distances up to 3.350 Å An additional eight atoms Sn2 (16*f*) at a distances up to 3.62 Å in the Ru_3Sn_7 complete the coordination polyhedron around Sn1 (12*d*) (CN = 16) (Figure 6c). In the $Sm_2Ru_3Sn_5$, the four samarium atoms approach the central of Sn1 (12*d*) atom at distances of 3.44 Å, and four Sn2 (8*c*) atoms from the former Sn2 (16*f*) site are removed at distances greater than 4 Å, and are not included in the coordination polyhedron of the Sn1 (12*d*) atom (Figure 6d). Interatomic distances in Ru_3Sn_7 between Sn1 (12*d*) and nearest neighbouring atoms in the polyhedron are Sn1-Sn2 3.62 Å, Sn1-Sn1 3.31 Å, Sn1-Ru 2.76 Å [42] (Figure 6c).

Coordination polyhedron of tin atom Sn2 (16*f*) in Ru_3Sn_7 compound is similar to those of Sm (8*c*) in $Sm_2Ru_3Sn_5$. It can be considered as a distorted hexagonal prism with one additional atom (3Ru + 4Sn1 + 6Sn2), CN = 13. The interatomic distances in the polyhedron range from 2.75 Å to 3.62 Å (Figures 3a and 6e). On the contrary, in the $Sm_2Ru_3Sn_5$

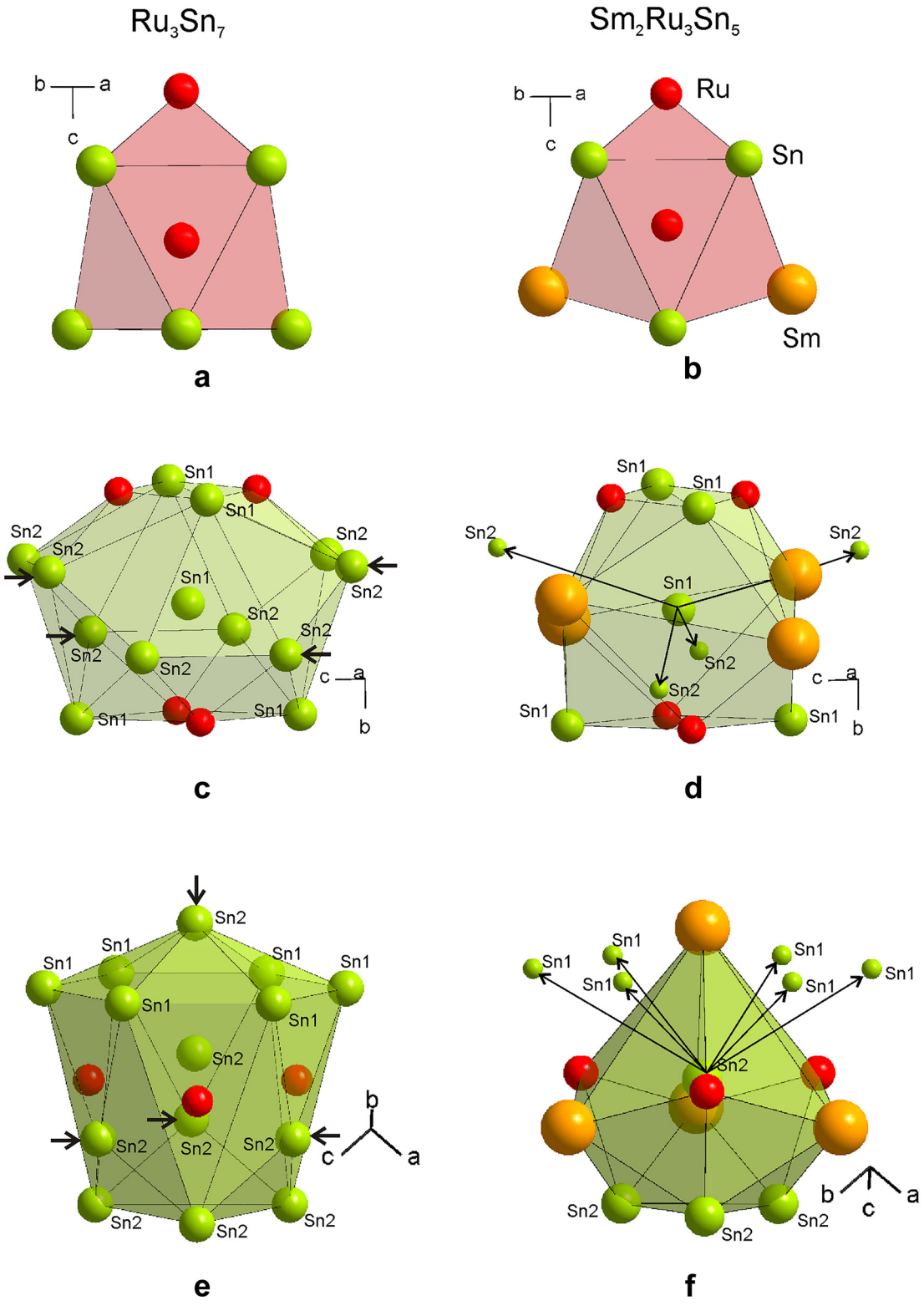

Figure 6: Left column: coordination polyhedra around Ru, Sn1, and Sn2 atoms in binary Ru_3Sn_7 structure, constructed according to the data [41, 42] (for Sn2 atom the atomic environment is expanded up to 4.27 Å). The arrows indicate those neighboring Sn2 atoms which are being replaced by Sm atoms in the corresponding polyhedra in $Sm_2Ru_3Sn_5$ structure. Right column: coordination polyhedra around Ru, Sn1 and Sn2 atoms in the new $Sm_2Ru_3Sn_5$ compound. In the right column, the small green balls are tin atoms squeezed out of the first coordination spheres in the $Sm_2Ru_3Sn_5$ structure.

structure, another coordination environment is formed around Sn2 (8*c*) atom, and is not similar to the coordination polyhedron of the Sn2 (16*f*) atom of the Ru_3Sn_7 binary intermetallic (Figures 3e and 6f). Under incorporation of samarium into the structure, coordination polyhedron at 8*c* site for Sm atoms in $Sm_2Ru_3Sn_5$ is a distorted hexagonal prism with one additional atom, and for Sn2 at 8*c* site is a 10-vertexes polyhedron (Figure 6f). Six Sn1 atoms are removed from the Sn2 (8*c*) environment at a distance of more than 4 Å, and three Sn2 atoms approach at a distance of 3.10 Å, while in the Ru_3Sn_7 structure they were 4.27 Å away from the central atom. Significant changes in the interatomic distances in the $Sm_2Ru_3Sn_5$ structure around the Sm and Sn2 atoms in the 8*c* positions become especially noticeable when compared with the corresponding distances around Sn2 (16*f*) in the Ru_3Sn_7 structure. It can be assumed that this is caused not only by the difference in the sizes of atoms Sm and Sn (1.80 and 1.40 Å [47]), but also by the different numbers of valence electrons.

In the studied structures, it is interesting to consider flat hexagonal atomic networks located in the mirror reflection plane (*m*) of the unit cell, because in ternary compounds $Nb_3Sb_2Te_5$ and $Sm_2Ru_3Sn_5$, all the atoms that replace the tin atoms in the prototype Ru_3Sn_7 are in this plane. The changes made to the structure are clearly traced in the corresponding flat grid (Figure 7). As can be seen from Figure 7, Ru and Sn (16*f*) atoms in Ru_3Sn_7 (Figure 7a), Nb, Sb (8*c*), and Te (8*c*) atoms in $Nb_3Sb_2Te_5$ (Figure 7b), as well as Ru, Sm (8*c*), and Sn (8*c*) atoms in $Sm_2Ru_3Sn_5$ (Figure 7c) form two types of conjugated hexagonal cells with *para*- and *ortho*-positions of Ru (Nb) atoms in them. The hexagonal networks in the Ru_3Sn_7 and $Nb_3Sb_2Te_5$ structures (Figure 7a and b) are practically undistorted, despite the absence of a center of symmetry and the appearance of a third type of atoms in the telluride compound. The absence of significant distortion of the networks in $Nb_3Sb_2Te_5$ is due to the close size of the atoms in the 8*c* positions. On the contrary, in the networks of the $Sm_2Ru_3Sn_5$ structure, a significant deviation from hexagonality is observed due to the introduction of larger samarium atoms (Figure 7c) instead of tin atoms. Replacing some of the tin atoms in the prototype with larger samarium atoms does not violate the flatness of the grids, while all the interatomic distances and angles in them change. In addition, the substitution with larger samarium atoms enforces an expansion of the unit cell compared to the prototype cell.

All distances from samarium to the nearest atoms are greater than to the corresponding atoms in Ru_3Sn_7. At the same time, the Ru-Ru and Ru-Sn distances in networks of the $Sm_2Ru_3Sn_5$ structure are slightly reduced. The Sm-Ru interatomic distances in the $Sm_2Ru_3Sn_5$ structure increase by more than 0.28 Å and are 3.03 Å compared to the corresponding Sn2-Ru values of 2.75 Å in the Ru_3Sn_7 structure (Table 3). Interatomic distance Sm-Sn2 is equal to 3.00 Å and corresponding distance Sn2-Sn2 in the Ru_3Sn_7 is 2.89 Å. In addition, in the binary compound Ru_3Sn_7, the interatomic distance for the Ru-Ru pair is 2.90 Å. In the non-centrosymmetric structure of $Sm_2Ru_3Sn_5$, the Ru–Ru distance in the ruthenium coordination polyhedron shortens and equal to 2.84 Å (Table 3).

Formally the structure of $Sm_2Ru_3Sn_5$ could be attributed to the structural type $Nb_3Sb_2Te_5$ on the basis of the similarity of the space group, the occupation of atomic positions and the proximity of the parameters of the unit cell. However, an analysis of the interatomic distances and the nearest environment of the atoms in each structure shows that the $Sm_2Ru_3Sn_5$ structure exhibits structural features that are differ from the centrosymmetric double Ru_3Sn_7 (Ir_3Ge_7) and from the non-centrosymmetric ternary $Nb_3Sb_2Te_5$ compound due to the different sizes of the atoms that make up the compound.

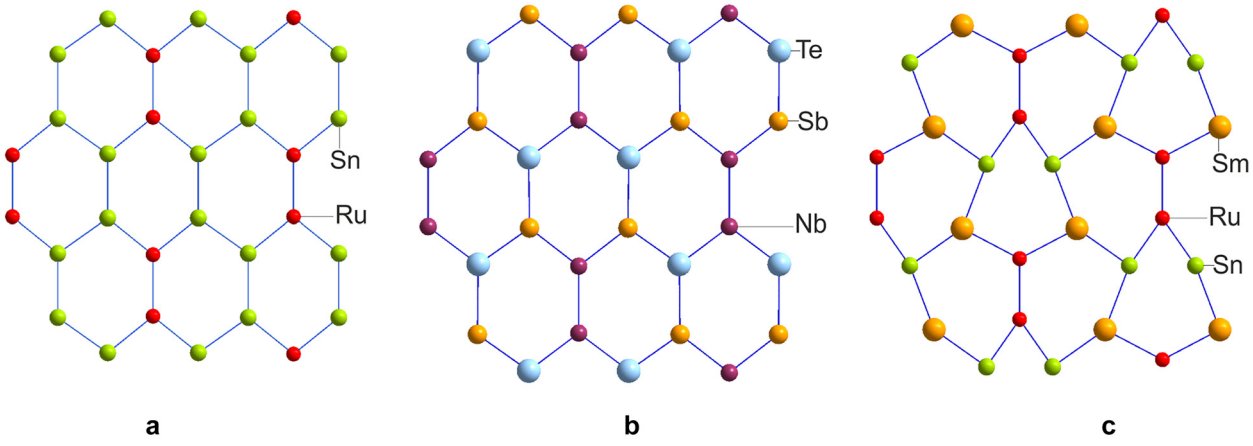

Figure 7: Hexagonal atomic networks in Ru_3Sn_7 (a); in $Nb_3Sb_2Te_5$ (b), in $Sm_2Ru_3Sn_5$ (c).

4 Conclusions

New samarium intermetallic compound $Sm_2Ru_3Sn_5$ crystallizes in a structure of the $Nb_3Sb_2Te_5$ type with cubic unit cell. The structure can be represented as related to the binary intermetallic structure of Ru_3Sn_7 with a loss of inversion center and an ordered distribution of Sm and Sn atoms in the two independent crystallographic positions.

Acknowledgements: The experimental data for X-ray structure analysis were obtained using equipment at the Shared Physical Characterization Facilities Center, Kurnakov Institute of General and Inorganic Chemistry, Russian Academy of Sciences.
Author contribution: All the authors have accepted responsibility for the entire content of this submitted manuscript and approved submission.
Research funding: The authors are thankful to the Russian Foundation for Basic Research (RFBR) for financial support (Grant No. 19-03-00135-a).
Conflict of interest statement: The authors declare no conflicts of interest regarding this article.

References

1. Biswas P. K., Balakrishnan G., Paul D. Mc. K., Lees M. R., Hillier A. D. *Phys. Rev. B* 2011, *83*, 054517.
2. Sung N. H., Roh C. J., Kim K. S., Cho B. K. *Phys. Rev. B* 2012, *86*, 224507.
3. Schmidt H., Müller M., Braun H. F. *Phys. Rev. B* 1996, *53*, 12389.
4. Singh Y., Ramakrishnan D. P. S., Awasthi A. M., Malik S. K. *Phys. Rev. B* 2005, *71*, 045109.
5. Ibrahim I. A. *J. Comput. Chem.* 2017, *38*, 2475–2480.
6. Sarkar S., Subbarao U., Joseph B., Peter S. *J. Solid State Chem.* 2015, *225*, 181–186.
7. Kussmann D., Pöttgen R., Kotzyba G. *J. Solid State Chem.* 2000, *150*, 112–120.
8. Kaczorowski D., Pikul A. P., Burkhardt U., Schmidt M., Slebarski A., Szajek A., Werwinski M., Grin Yu. *J. Phys. Condens. Matter* 2010, *22*, 215601.
9. Godart C., Gupta L., Tomy C., Patil S., Nagarajan R., Beaurepaire E., Vijayaraghavan R., Yakhmi J. *Mater. Res. Bull.* 1988, *23*, 1781.
10. Anand V., Hossain Z., Geibel C. *Phys. Rev. B* 2008, *77*, 184407.
11. Singh Y., Ramakrishnan S., Hossain Z., Geibel C. *Phys. Rev. B* 2002, *66*, 014415.
12. Hossain Z., Ohmoto H., Umeo K., Iga F., Suzuki T., Takabatake T., Takamoto N., Kindo K. *Phys. Rev. B* 1999, *60*, 10383.
13. Anand V., Anupam K., Hossain Z., Ramakrishnan S., Thamizhavel A., Adroja D. *J. Magn. Magn Mater.* 2012, *324*, 2483–2487.
14. Yarmolyuk Y., Aksel'rud L. *Sov. Phys. Crystallogr.* 1977, *22*, 358–359.
15. Akselrud L., Yarmolyuk Y., Gladyshevskii E. *Sov. Phys. Crystallogr.* 1977, *22*, 492–493.
16. Gorelenko Y., Skolozdra R., Dutchak Y., Yarovets V., Shcherba I., Bodak O. *Ukr. Fiz. Zh.* 1985, *30*, 301–304.
17. Méot Meyer M., Venturini G., Malaman B., Steinmetz J., Roques B. *Mater. Res. Bull.* 1984, *19*, 1181–1186.
18. Pöttgen R., Lang A., Hoffmann R. D., Künnen B., Kotzyba G., Müllmann R., Mosel B. D., Rosenhahn C. *Z. Kristallogr.* 1999, *214*, 143–150.
19. Galadzhun Y., Hoffmann R.-D., Pöttgen R., Adam M. *J. Solid State Chem.* 1999, *148*, 425–432.
20. Sebastian C., Salvador J., Martin J., Kanatzidis M. *Inorg. Chem.* 2010, *49*, 10468–10474.
21. Bugaris D. E., Malliakas C. D., Bud'ko S. L., Calta N. P., Chung D. Y., Kanatzidis M. G. *Inorg. Chem.* 2017, *56*, 14584–14595.
22. Fukuhara T., Sakamoto I., Sato H. *J. Phys. Condens. Matter* 1991, *3*, 8917.
23. Fukuhara T., Iwakawa S., Sato H. *J. Magn. Magn Mater.* 1992, *104*, 667–668.
24. Godart C., Mazumdar C., Dhar S., Flandorfer K., Nagarajan R., Gupta L., Vijayaraghavan R. *Europhys. Lett.* 1994, *27*, 215.
25. Zumdick M. F., Pöttgen R. *Z. Naturforsch. B Chem. Sci.* 1999, *54*, 863–869.
26. Koch N. E., Strydom A. M. *J. Magn. Magn Mater.* 2008, *320*, 128–131.
27. Heying B., Kösters J., Hoffmann R. D., Heletta L., Pöttgen R. *Z. Naturforsch. B Chem. Sci.* 2017, *72*, 753–758.
28. Gamza M. B., Gumeniuk R., Burkhardt U., Schnelle W., Rosner H., Leithe-Jasper A., Slebarski A. *Phys. Rev. B* 2017, *95*, 165142.
29. Patil N., Ramakrishnan S. *Phys. Rev. B* 1999, *59*, 12054–12063.
30. Palenzona A., Canepa F. *J. Less Common. Met.* 1989, *155*, L31–L33.
31. Okamoto H. *J. Phase Equil.* 1991, *12*, 253–254.
32. Schwomma O., Nowotny H., Wittmann A. *Monatsh. Chem.* 1964, *95*, 1538–1543.
33. Shevchenko M. O., Berezutski V. V., Ivanov M. I., Kudin V. G., Sudavtsova V. S. *J. Phase Equilibria Diffus.* 2015, *36*, 39–52.
34. Sheldrick G. M. *XPRER 6.14, Bruker Saint*. BRUKER APEX 2016, *3*.
35. Sheldrick G. M. *Sadabs – Bruker Nonius Area Detector Scaling and Absorption Correction*; Univesity of Göttingen: Germany, 2004.
36. Sheldrick G. M. *Acta Crystallogr.* 2015, *C71*, 3–8.
37. Stoe Winxpow (Version 2.24). Stoe & Cie GmbH, Germany, Darmstadt, 2009.
38. Rodriguez-Carvajal J. *Phys. B* 1993, *192*, 55–69.
39. Roisnel T., Rodriguez-Carvajal J. *Mater. Sci. Forum* 2000, 118–123.
40. Brandenburg K. *Diamond. Release 3.0*; Crystal Impact Gmbh: Bonn, Germany, 2005.
41. Nowotny H. N., Schubert K. Dettinger U. *Metallforschung* 1946, *1*, 137–145.
42. Bryan C., Mandrus D. *J. Alloys Compd.* 1998, *281*, 157–159.
43. Spek A. L. PLATON. *Acta Crystallogr. A* 2009, *D65*, 148–155.
44. Eriksson L., Lanner J. *Acta Crystallogr.* 2001, *E57*, 185–186.
45. Jensen P., Kjekshus A. *J. Less Common. Met.* 1967, *13*, 357–359.
46. Soheilnia N., Giraldi J., Assoud A., Zhang H., Tritt T., Kleinke H. *J. Alloys Compd.* 2008, *448*, 148–152.
47. Emsley J. *The Elements*; Clarendon Press: Oxford, 1991.
48. Bärnighausen H. *Commun. Math. Chem.* 1980, *9*, 139–175.
49. Müller U. *Z. Anorg. Allg. Chem.* 2004, *630*, 1519–1537.